

Pick, break, and placement of one-dimensional nanostructures for direct assembly and integration

Brian D. Sosnowchik,^{a)} Jiyoung Chang, and Liwei Lin

Department of Mechanical Engineering, Berkeley Sensor and Actuator Center, University of California, Berkeley, California 94720, USA

(Received 4 November 2009; accepted 26 February 2010; published online 12 April 2010)

A direct, simple, and versatile assembly method for the manipulation of one-dimensional nanostructures and their integration with microscale devices has been demonstrated. Using a probe station with an unbiased tungsten probe, the facile process has been employed to accurately pick, break, and place individual titanium dioxide nanoswords and zinc oxide nanowires under a room-temperature, dry environment. The surface morphology of the nanostructures, probe tips, and adhesion forces were characterized. As such, the technique could enable the rapid assembly of individual nanostructures with complementary metal-oxide-semiconductor-compatible or complex microscale devices. © 2010 American Institute of Physics. [doi:10.1063/1.3374879]

One of the fundamental challenges in the field of micro and nanotechnology is the ability to manipulate and assemble structures at the micro or nanoscale. Much of the difficulty is due, in part, to the size scale of the materials and the inability to precisely manipulate them. As such, a variety of techniques have been developed to circumvent these issues, classified by their approach to manipulation and size-scale of assembly. The first category employs passive nanostructure manipulation, suitable for large-scale assembly, including contact printing,¹ and dielectrophoretic techniques.² However, for these approaches, the manipulation of nanostructures is enabled through the use of specially processed substrates and precise assembly of *single* nanostructures remains nonpractical. The second category employs direct manipulation techniques, enabling individual nanostructure assembly and including methods like optical trapping,³ atomic force microscopy (AFM),⁴ and microfabricated tweezer-probes.⁵ However, most of these techniques, though elegant, require complicated experimental approaches or equipment.

Herein, we present a simple, fast, and direct manipulation and integration technique to “pick,” “break,” and “place” individual nanostructures in a single operation using a widely available tungsten probe tip installed on micromanipulator under an optical probe station. The technique presented is versatile, quick, simple, may be performed without a fluidic medium⁶ or elaborate substrates,⁷ and may be used for rapid nanostructure characterization and the creation of functional nanodevices that would be challenging using other assembly methods.

Figure 1(a) illustrates the process to pick, break, and place one-dimensional (1D) nanostructures, enabling their integration with target substrates. Titanium dioxide (TiO₂) nanoswords, first discovered by our group,⁸ are shown as an example. First, a standard tungsten probe tip contacts a nanosword protruding from a growth substrate as visualized under an optical microscope and bends the one-dimensional (1D) nanostructure. When the stress at the base of the nanosword becomes large enough, the nanostructure breaks free from the growth substrate and remains on the probe tip. The

nanostructure may be subsequently positioned onto a target substrate, completing the integration process. In contrast to all aforementioned methodologies, this technique is fast and simple to pick, break, and place individual nanostructures in a single assembly operation.

The underlying principle of the proposed technique depends on the net attractive forces and contact area between two objects. As the separation distance between two objects is reduced to the nanoscale, surface tension, van der Waals and electrostatic forces have been shown to dominate nanostructure adhesion.⁹ For two dry, unbiased flat surfaces, the adhesion force per area, f_{LJ} , can be modeled by the Lennard-Jones (LJ) interaction potential as,¹⁰

$$f_{LJ}(z) = 8\Delta\gamma/3z_0[(z_0/z)^3 - (z_0/z)^9], \quad (1)$$

where z_0 is the equilibrium separation distance. Likewise, the surface energy, $\Delta\gamma$, may be determined with the Hamaker constant, A , of the materials as,

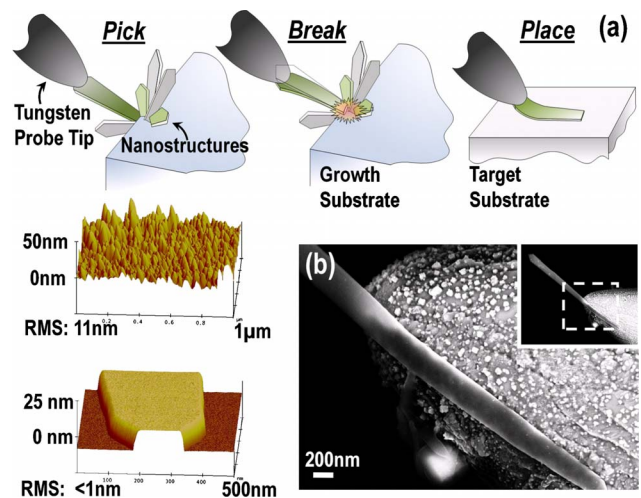


FIG. 1. (Color online) (a) Schematic of the “pick,” “break,” and “placement” technique. (b) Probe tip with an attached nanosword. The surface is visibly roughened with an RMS of 11 nm, while the nanosword on polished silicon is smooth.

^{a)}Electronic mail: bdsosnow@me.berkeley.edu.

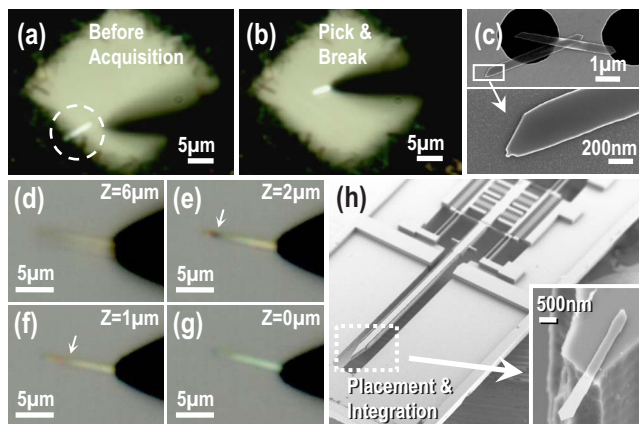


FIG. 2. (Color online) Encircled nanostructure in (a) is contacted by the unbiased tungsten probe tip breaking the nanostructure (b) at the tapered base (c). Changes in the optical interference gratings (d)–(g) provide visual feedback of the nanostructure-substrate gap. (h) Contact is made, and the nanosword remains cantilevered as positioned.

$$\Delta\gamma = A/16\pi z_o^2. \quad (2)$$

To illustrate the working principle, TiO_2 nanoswords (lengths of 3–10 μm , widths of 200–1000 nm, and thicknesses of 40–80 nm) and zinc oxide (ZnO) nanowires (75–125 nm in diameter and lengths of 9–12 μm) were rapidly synthesized using the previously reported induction heating platform^{11,12} for a duration of several minutes. The Cascade Microtech tungsten probe tips used in this work had a sharpness of 2.4 μm . Figure 1(b) shows an image of the tungsten probe tip with a nanosword attached to the visibly roughened tip. Tapping mode AFM was used to visualize the surface morphology of the probe tip. The three-dimensional rendering of the root mean squared (RMS) surface roughness 3 μm from the probe tip was measured to be 11 nm. A scan was also taken along the surface of the nanosword on a polished silicon substrate, where the rms roughness was measured to be <1 nm, similar to the silicon surface.

The nanoswords for this work were grown on copper transmission electron microscopy grids. When observed with an optical microscope at 1000 \times magnification, Fig. 2(a) shows the clearly visible, protruding nanostructures. Acquisition occurs when the tungsten probe tip initiates contact with the encircled nanosword, bending and ultimately breaking the nanosword away from the growth substrate at the base, as shown in Fig. 2(b). Because the nanosword bases are tapered [Fig. 2(c)], the stress induced at the interface from modest bending distances is sufficient to fracture the interfacial contact. Figures 2(d)–2(g) demonstrate nanosword positioning onto silicon with a 100 nm thermally-grown oxide layer, as imaged with the tip of the probe located 6, 2, 1, and 0 μm above the surface of the substrate. As the nanosword comes into focus in Fig. 2(d), optical interference gratings appear on the surface of the nanosword, shown at the arrowhead of Fig. 2(e). Changes in the optical interference gratings provide qualitative visual feedback of the gap between the nanosword and the substrate. With further probe descent in Fig. 2(f), the dark spot at the arrowhead shifts along the nanosword toward the probe tip, indicating a reduction of the nanosword-substrate gap. The gratings ultimately disappear when the nanosword contacts the substrate [Fig. 2(g)], allowing the placement of nanostructures on a variety of different materials and architectures [Fig. 2(h)]. The overall process

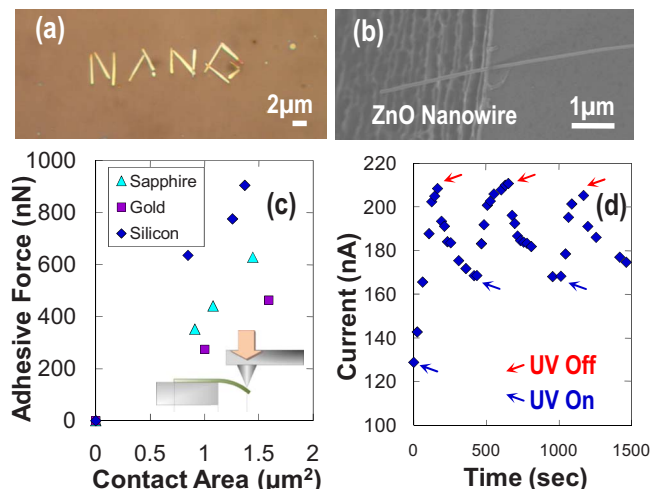


FIG. 3. (Color online) Several key demonstrations, a characterization, and application of the technique. Assembly of (a) the word “NANO” with nanoswords and (b) placement of a single ZnO nanowire (c) Contact-mode AFM was used to quantify the nanosword adhesive force for various substrates. (d) Sensitivity of a single nanosword to ultraviolet light.

may be accomplished in about 30 s with manual operation, with the majority of time spent on global stage and probe tip movement. Figures 3(a) and 3(b) show several key examples demonstrating the versatility of this technique including the assembly of the word “NANO” on oxidized silicon using twelve nanoswords, and the placement of a ZnO nanowire on the edge of a silicon-on-insulator device.

To quantify the adhesive forces of the nanosword to the surface materials, contact-mode AFM was used to apply a moment to a fixed-free cantilevered nanosword on various substrates. The moment was incrementally increased and eventually overcame the adhesion force, at which point the nanosword fell off of the substrate and the moment data were recorded. Test specimens were first prepared on the following substrates: (1) piranha-cleaned, p-type (B), 10–50 Ωcm , $\langle 100 \rangle$ silicon, (2) piranha-cleaned, c-plane sapphire, and (3) silicon with a 5 nm/20 nm Cr/Au evaporated thin film. The spring constants of the rectangular cross-section AFM cantilevers were calibrated using the method by Sader *et al.*,¹³ and it was assumed that the adhesion force was constant across the entire effective contact area with no slip. The moment data were used with Eq. (3) to quantify the adhesive force per area, f_{adh} ,

$$f_{\text{adh}} = F_{\text{AFM}}a/bA_{\text{adh}}, \quad (3)$$

where F_{AFM} is the applied force, a is the moment arm, A_{adh} is the estimated nanosword-substrate contact area, and b is the edge-to-centroid distance. Scanning electron microscope (SEM) images were taken of the cantilevered nanoswords, and the centroids and contact areas were calculated from the digitized perimeter. Figure 3(c) illustrates the nanosword adhesion data. The data show a linear dependence of the adhesive force with respect to the nanosword contact area. Silicon showed the greatest adhesion force, followed by sapphire and gold, with the linear slope of the data reflecting a constant adhesion force per area of 658, 417, and 287 $\text{nN}/\mu\text{m}^2$, respectively. Since both the acquisition and placement processes were possible in a dry environment when electrically grounding the probe, the target, and the growth substrates, the conductive nanostructures are assumed to be charge neu-

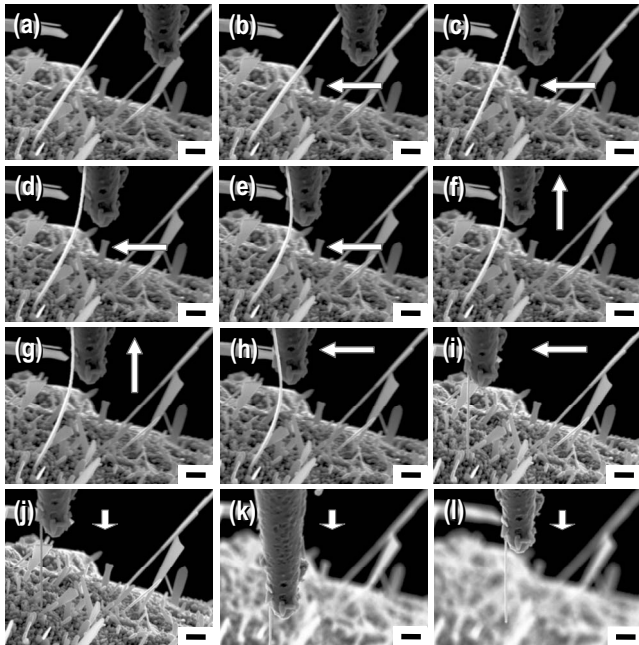


FIG. 4. *In situ* SEM study of the nanostructure acquisition using Kleindiek piezoelectric-actuated micropositioner. Scale bars are 500 nm.

tral, and van der Waals forces are assumed to dominate adhesion. Therefore, Eq. (1) may be used to calculate the theoretical adhesion force. Hamaker constants of 6.9 and 31 zJ have been reported for TiO_2 on silicon and sapphire substrates, respectively.¹⁴ Likewise, roughnesses of 0.14 nm, 0.19 nm, and 1.7 nm were measured by AFM for the nanosword, silicon, and sapphire, respectively. Assuming that the surfaces are coated by a monolayer of adsorbed water (0.35 nm),¹⁵ the theoretical force per area is calculated to be 556 and 381 $\text{nN}/\mu\text{m}^2$ at separation distances of 0.87 nm and 1.63 nm for the silicon and sapphire substrates, respectively, which are comparable to the experimental values. It should be noted that although a value for the Hamaker constant of TiO_2 on gold could not be found, the increased surface roughness of the gold substrate may result from grain formation in the layer, weakening the adhesion force.

To show a device demonstration of the technique, an ultraviolet (UV) light sensor was characterized by positioning an individual nanosword and fabricating Cr/Au electrodes. The output current was monitored under a 1 V bias with 6 W UV at 365 nm. Figure 3(d) show the repeatable 25% increase in the output current. This technique was also used for the fabrication plasmonic antennas for surface enhanced Raman spectroscopy (SERS) detection.¹⁶

A Zeiss field-emission SEM equipped with a Kleindiek piezoelectric-actuated micropositioner with a tungsten probe (PTT-70–25/Cascade) was used to analyze the nanosword acquisition process. Figure 4(a) illustrates the probe initially in the plane of the nanosword. As the probe moved to the left in Figs. 4(b) and 4(c), the tip of the nanosword slid along the surface of the probe, stopped eventually by friction. The probe was moved further to the left in Figs. 4(d) and 4(e), increasing the effective contact of the nanosword with the probe. Subsequently, the probe was moved in plane away from the growth substrate for two reasons—to reduce axial compression of the nanosword and to inspect its release from the substrate. The former was achieved in Fig. 4(f), further

increasing the bending stress at the base. However, the reduction of the nanosword-probe contact area evident from Figs. 4(f) and 4(g) indicated that the base had not yet been broken. Because of this, the probe was moved further to the left in Fig. 4(h). With an eventual vertical realignment with the nanosword in Fig. 4(i), the nanosword was broken away from the growth substrate, shown in Figs. 4(j)–4(l).

The work presented herein represents a simple and practical approach for the manipulation and integration of individual 1D nanostructures with other systems, and may be characterized as follows. The technique is room-temperature, dry and versatile, with a positioning accuracy of $\sim 1 \mu\text{m}$ and an acquisition yield of 90%. Once positioned, the probe tip may be used to refine the nanostructure orientation, an example of which was demonstrated with alignment down to 70 nm.¹⁶ By monitoring changes in the optical interference patterns, placement pressure from the probe tip may be minimized, thus enabling assembly on fragile structures, like the 50 nm thick silicon nitride membranes in Fig. 2(c). Furthermore, the LJ model reflects the significance of separation distance, and it is believed that use of vacuum conditioning may result in significant adhesion improvement compared to the measured values. Several limiting characteristics of the system include the need for optically visible nanostructures, with flat, defined facets, and smooth target substrates to increase the effective contact area with a small nanostructure-substrate separation distance. However, the current technique is fast, and it is believed that use of an automated pick-and-place platform similar to that for chip-based integration could enable a rapid means to assemble individual nanostructures into complementary metal-oxide-semiconductor-compatible or microelectromechanical systems devices.¹⁷

¹Z. Fan, J. C. Ho, Z. A. Jacobson, R. Yerushalmi, R. L. Alley, H. Razavi, and A. Javey, *Nano Lett.* **8**, 20 (2008).

²P. A. Smith, C. D. Nordquist, T. N. Jackson, T. S. Mayer, B. R. Martin, J. Mbindyo, and T. E. Mallouk, *Appl. Phys. Lett.* **77**, 1399 (2000).

³A. Jamshidi, P. J. Pauzauskie, P. J. Schuck, A. T. Ohta, P.-Y. Chiou, J. Chou, P. Yang, and M. C. Wu, *Nat. Photonics* **2**, 85 (2007).

⁴W. L. Hughes and Z. L. Wang, *Appl. Phys. Lett.* **86**, 043106 (2005).

⁵K. Mølhave, T. Wich, A. Kortschack, and P. Boggild, *Nanotechnology* **17**, 2434 (2006).

⁶K. Reynolds, J. Komulainen, J. Kivijakola, P. Lovera, D. Iacopino, M. Pudas, J. Vahakangas, J. Roning, and G. Redmond, *Nanotechnology* **19**, 485301 (2008).

⁷Q. Li, S.-M. Koo, C. A. Richter, M. D. Edelstein, J. E. Bonevich, J. J. Kopanski, J. S. Suehle, and E. M. Vogel, *IEEE Trans. NanoTechnol.* **6**, 256 (2007).

⁸B. D. Sosnowchik, J.-Y. Ha, L. Luo, and L. Lin, 21st IEEE Micro Electro Mechanical Systems Conference (IEEE, Tucson, AZ, 2008).

⁹R. S. Fearing, IEEE/RSJ International Conference on Intelligent Robots and Systems (IEEE, Pittsburgh, PA, 1995).

¹⁰V. M. Muller, V. S. Yushchenko, and B. V. Derjaguin, *J. Colloid Interface Sci.* **77**, 91 (1980).

¹¹B. D. Sosnowchik and L. Lin, *Appl. Phys. Lett.* **89**, 193112 (2006).

¹²L. Luo, B. D. Sosnowchik, and L. Lin, *Appl. Phys. Lett.* **90**, 093101 (2007).

¹³J. E. Sader, J. W. M. Chon, and P. Mulvaney, *Rev. Sci. Instrum.* **70**, 3967 (1999).

¹⁴L. Bergstrom, *Adv. Colloid Interface Sci.* **70**, 125 (1997).

¹⁵J. M. Thorp, *Trans. Faraday Soc.* **55**, 442 (1959).

¹⁶B. D. Sosnowchik, P. J. Schuck, J. Chang, and L. Lin, 22nd IEEE Micro Electro Mechanical Systems Conference (IEEE, Sorrento, Italy, 2009).

¹⁷See supplementary material at <http://dx.doi.org/10.1063/1.3374879> for additional system characterizations, movies, sample preparation, and AFM testing.